JCI The Journal of Clinical Investigation

The IRE1α/XBP1 pathway sustains cytokine responses of group 3 innate lymphoid cells in inflammatory bowel disease

Siyan Cao, … , Parakkal Deepak, Marco Colonna

J Clin Invest. 2024. https://doi.org/10.1172/JCI174198.

Research In-Press Preview Gastroenterology Immunology

Graphical abstract

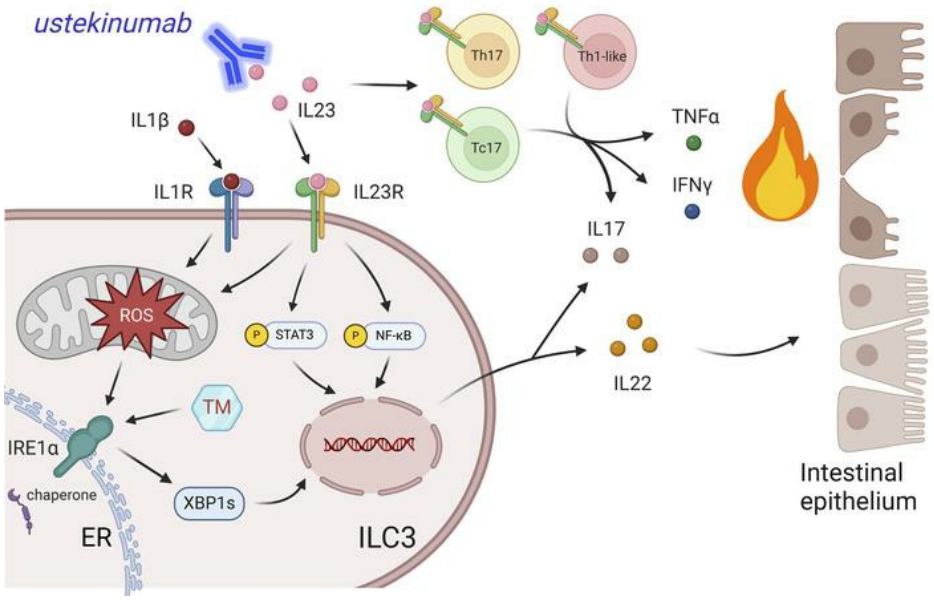

The IRE1α/XBP1 pathway sustains cytokine responses of group 3 innate lymphoid cells in inflammatory bowel disease

Authors: Siyan Cao[1,2], Jose L. Fachi[2], Kaiming Ma[1], Alina Ulezko Antonova[2], Qianli Wang[2], Zhangying Cai[2], Randal J. Kaufman[3], Matthew A. Ciorba[1], Parakkal Deepak[1], Marco Colonna[2]*

[1]Division of Gastroenterology, Department of Medicine, Washington University School of Medicine, St. Louis, MO 63110.

[2]Department of Pathology and Immunology, Washington University School of Medicine, St. Louis, MO 63110.

[3]Degenerative Diseases Program, Center for Genetic Disorders and Aging Research, Sanford Burnham Prebys Medical Discovery Institute, La Jolla, CA 92037.

*Correspondence: Marco Colonna, Washington University in St Louis, 660 S. Euclid Ave, St. Louis, MO 63110, USA. Phone number: (314) 362-0367. Email: mcolonna@wustl.edu.

Conflict-of-interest statement

Marco Colonna, MD received research grants from Aclaris Therapeutics, unrelated to the data in the study. Matthew Ciorba, MD has received grants unrelated to the current content from AbbVie, Takeda, Pfizer, and Janssen. Parakkal Deepak, MBBS MS received research support under a sponsored research agreement unrelated to the data in the study and/or consulting from AbbVie, Arena Pharmaceuticals, Boehringer Ingelheim, Bristol Myers Squibb, Janssen, Pfizer, Prometheus Biosciences, Takeda Pharmaceuticals, Roche Genentech, Scipher Medicine, Fresenius Kabi, Teva Pharmaceuticals, Landos Pharmaceuticals, Iterative scopes and CorEvitas, LLC.

ABSTRACT

Group 3 innate lymphoid cells (ILC3s) are key players in intestinal homeostasis. Endoplasmic reticulum (ER) stress is linked to inflammatory bowel disease (IBD). Herein, we used cell culture, mouse models, and human specimens to examine if ER stress in ILC3s impacts IBD pathophysiology. We show that mouse intestinal ILC3s exhibited a 24h-rhythmic expression pattern of the master ER stress response regulator, IRE1α/XBP1. Proinflammatory cytokine IL-23 selectively stimulated IRE1α/XBP1 in mouse ILC3s through mitochondrial reactive oxygen species (mtROS). IRE1α/XBP1 was activated in ILC3s of mice exposed to experimental colitis and in inflamed human IBD specimens. Mice with *Ire1α* deletion in ILC3s (*Ire1α*$^{\Delta Rorc}$) showed reduced expression of ER stress response and cytokine genes including *Il22* in ILC3s and were highly vulnerable to infections and colitis. Administration of IL-22 counteracted their colitis susceptibility. In human ILC3s, IRE1 inhibitors suppressed cytokine production, which was upregulated by an IRE1 activator. Moreover, the frequencies of intestinal XBP1s^{+} ILC3s in Crohn's disease patients before administration of ustekinumab, an anti-IL-12/IL-23 antibody, positively correlated with response to treatment. We demonstrate that a non-canonical mtROS-IRE1α/XBP1 pathway augments cytokine production by ILC3s and identify XBP1s^{+} ILC3s as a potential biomarker for predicting response to anti-IL-23 therapies in IBD.

Introduction

Innate lymphoid cells (ILCs) are a group of immune cells that exhibit lymphoid characteristics yet lack antigen-specific receptors found on T and B cells (1). Group 3 ILCs (ILC3s) comprise the most abundant ILC population in the intestine. ILC3s require the master transcription factor RORγt for their development and secrete IL-22, IL-17 and in humans only, IL-26. Hence, ILC3s are the innate counterparts of Th17 cells. ILC3 cytokine secretion follows a circadian oscillation (2, 3) and is stimulated by IL-23, IL-1β, and IL-18, which are released by intestinal epithelial and myeloid cells in response to intestinal bacteria, nutritional components, and other environmental stimuli. Through secretion of IL-22, IL-17, and IL-26, ILC3s sustain the protective functions of epithelial, stromal, and myeloid cells, heightening epithelial barrier integrity. They also maintain intestinal tolerance to microbiota and prevent autoimmunity through induction of microbiome-specific regulatory T cells (4, 5). Accordingly, several studies reported that ILC3s are diminished in inflamed tissue of inflammatory bowel diseases (IBD) (6, 7). However, inappropriate activation of ILC3s can also promote inflammation and contribute to the physiopathology of IBD. Supporting this observation, IBD risk alleles, such as *RORC*, *IL23R*, *IL22*, *IL17A*, and *IL26* (8, 9), are not only expressed in pathogenic Th17 cells but also in ILC3s. Because of the potential relevance of ILC3s in human IBD, it is essential to fully determine the regulatory mechanisms controlling ILC3s in intestinal inflammation.

In eukaryotic cells, the endoplasmic reticulum (ER) plays a crucial role in folding and post-translational modifications of all membrane proteins and most secreted proteins (10). This intricate process is highly sensitive to changes in both the cell's internal and external environments. When disturbances occur, leading to the accumulation of unfolded or misfolded proteins within the ER lumen, a condition known as ER stress arises. ER stress triggers a complex cellular response called the unfolded protein response (UPR), which regulates various aspects of cell function, proliferation, and survival. In mammalian cells, ER stress activates three main protein sensors located on the ER membrane, namely inositol-requiring kinase 1 (IRE1),

pancreatic ER eIF2α kinase (PERK), and activating transcription factor 6 (ATF6). Among these sensors, IRE1α stands out as the most conserved, possessing both a serine/threonine kinase domain and an endoribonuclease domain within its cytosolic portion. Upon activation, IRE1α cleaves a specific mRNA known as X-box-binding protein 1 (XBP1), generating a spliced isoform (XBP1s). This XBP1s protein acts as a potent transcription factor, regulating numerous cellular processes including mRNA translation within the ER, protein folding and maturation, immune and inflammatory responses, as well as anti-apoptotic signaling (10-12).

Numerus stimuli induce ER stress in the gastrointestinal tract, impacting key processes in immune and non-immune cells (13-22). Furthermore, *XBP1* variants including nonsynonymous SNPs are associated with IBD (13). Whether ER stress influences ILC3 function has not been investigated. Here, we found that mouse intestinal ILC3s express IRE1α and that its downstream product *Xbp1s* follows a robust circadian rhythm, which parallels that of *Il22* at steady state. The IRE1α/XBP1 pathway was activated *ex vivo* in response to stimulation with the neuropeptide VIP and the inflammatory cytokines IL-23 and IL-1β; such activation relied on mitochondrial reactive oxygen species (mtROS). IRE1α/XBP1 activation in ILC3s occurred in mice exposed to dextran sulfate sodium (DSS)-induced colitis, while intestinal specimens from IBD patients expressed higher XBP1s than did healthy controls. Using a conditional knockout mouse model in which *Ire1α* is deleted in ILC3s (*Ire1α*$^{\Delta Rorc}$ mice), we showed that mouse ILC3s required IRE1α/XBP1 for efficient production of IL-22 and IL-17. *Ire1α*$^{\Delta Rorc}$ mice were highly susceptible to colitis induced by *C. difficile* and *C. rodentium* as well as DSS-induced colitis; the latter was attenuated by administration of exogenous IL-22. In humans, cytokine production by ILC3s was attenuated by selective inhibitors of IRE1; conversely, an IRE1 activator potentiated ILC3 production of IL-22 in response to a very low concentration of IL-23. Finally, the pre-treatment frequency of XBP1s-expressing ILC3s in the intestine from Crohn's Disease (CD) patients positively correlated with their response to ustekinumab, an antagonist of the p40 subunit of IL-12/IL-23. We conclude that the IRE1α/XBP1 pathway sustains ILC3 production of cytokines that maintain intestinal

homeostasis. Since XBP1s activation in ILC3s is an indicator of the responsiveness to IL-23 in IBD patients, XBP1s^{+} ILC3s may be a useful biomarker to select a subset of IBD patients who may benefit from therapies that inhibit IL-23.

Results

Intestinal ILC3s exhibit high Ire1α expression and *circadian oscillation of Xbp1s*

We first examined whether ER stress pathways are activated in mouse ILC3s. We noted that *Ire1α* (*Ern1*) mRNA was highly expressed in ILC3s of the small intestinal lamina propria (siLP) compared to other cell populations in Immgen microarray and ULI RNA-seq data (Immgen.org) (**Figure 1A**). Previous studies demonstrated that the expression of prototypic ILC3 genes, such as *Il22*, follow a 24-hour circadian rhythm as do clock genes like *Period circadian regulator 1* (*Per1*) (2, 3, 23). Thus, we tested whether IRE1α/XBP1 expression also follows a cyclic oscillation in ILC3s at steady state. We sort-purified siLP ILC3s (**Supplemental Figure 1A**) from wild-type C57BL/6J mice every 6 hours over a 24-hour period for qPCR analysis of genes controlling ER stress response. Using JTK_CYCLE analysis, we found robust rhythmic expression of *Xbp1s* peaking at ZT12 over a 24-hour period, which paralleled that of *Il22* and *Per1* (**Figure 1B**). Circadian oscillations of *Pdi*, which encodes an ER protein disulfide isomerase, and *Bip*, an ER chaperone gene, were limited. We also observed cyclic expression of *Chop* (*Ddit3*, or DNA damage inducible transcript 3), which encodes a pro-apoptotic transcription factor during ER stress (11). However, the expression of *Chop* peaked at ZT0 when *Xbp1s*, *Per1* and *Il22* transcripts were at their nadir, suggesting that CHOP may counterbalance the activity of IRE1α/XBP1 pathway in intestinal ILC3s. Vasoactive intestinal peptide (VIP) is a neuropeptide produced by enteric neurons during feeding, which was previously shown to induce the rhythmic expression of ILC3 cytokines including IL-22 (24-26). We found that *ex vivo* treatment of siLP ILC3s with VIP or the VIP receptor agonist BAY 55-9837 upregulated XBP1s in siLP ILC3s

(**Figure 1C**). This finding suggests a strong connection between nutritional response and the circadian regulation of IRE1α/XBP1. Moreover, it implies that VIP secretion induced by food intake might regulate cytokine production in gut ILC3s via the IRE1α/XBP1 pathway.

ER stress enhances ILC3 production of cytokines

To directly investigate whether ER stress impacts cytokine production of ILC3s, we sorted siLP ILC3s from wild-type C57BL/6J mice (**Supplemental Figure 1A**). ILC3s were stimulated *ex vivo* with IL-23 plus IL-1β with or without tunicamycin (TM), a classical ER stress inducer that activates all three branches of the UPR (i.e., IRE1α, PERK, and ATF6). Stimulation of ILC3s with IL-23 plus IL-1β induced production of IL-22 and IL-17A, which were enhanced by co-treatment with TM (**Figure 2A, B; Supplemental Figure 1B, C**). Stimulation of ILC3s with TM alone had minimal impact on expression of cytokines (**Supplemental Figure 1C**). We conclude that ER stress enhances ILC3 cytokine production induced by proinflammatory cytokines.

ILC3s exposed to inflammatory cytokines, experimental colitis, and IBD selectively activate IRE1α/XBP1.

We further investigated the expression of the IRE1α/XBP1 pathway during ILC3 activation *ex vivo* and *in vivo*. We isolated siLP ILC3s, stimulated them *ex vivo* with IL-23 plus IL-1β or TM, and examined the intracellular content of XBP1s in ILC3s by flow cytometry. Stimulation of siLP ILC3s with either IL-23 plus IL-1β or TM induced similar expression of XBP1s, suggesting that inflammatory cytokines are sufficient to activate the IRE1α/XBP1 branch of the UPR pathway. Moreover, TM together with IL-23 and IL-1β had an additive effect (**Figure 2C**). We further examined the expression of ER stress genes in sorted siLP ILC3s by quantitative real-time PCR (qPCR). This analysis corroborated that IL-23 and IL-1β selectively activate the IRE1α/XBP1 branch of the UPR, but have a limited impact on the other two UPR branches - the PERK pathway (*Chop*) and ATF6 pathway (*Bip* and *Grp94*) (**Figure 2D**).

We next examined IRE1α/XBP1 activation in colonic ILC3s in the DSS-induced model of colitis. We collected cells from the colon lamina propria of mice on day 5 of DSS treatment and analyzed intracellular XBP1s in ILC3s by flow cytometry. The percentage of ILC3s expressing XBP1s was higher in mice with DSS colitis than untreated mice (**Figure 2E**). The expression of XBP1s remained unchanged in other ILC subsets—ILC1, ILC2, and NK cells—in the colon during DSS colitis (**Supplemental Figure 2**). Furthermore, we examined the frequencies of XBP1s^{+} ILC3s in inflamed intestinal biopsies from patients with CD or ulcerative colitis (UC), as well as normal mucosal tissues from healthy controls (n = 6 or 7 per group. **Figure 2F; Supplemental Figure 3**). The data indicated that IRE1α/XBP1 pathway in ILC3s is also activated in response to intestinal inflammation in patients with IBD.

IRE1α/XBP1 activation in ILC3s requires mitochondrial reactive oxygen species

We sought to elucidate the mechanism underpinning IRE1α/XBP1 activation in ILC3 during inflammation. It has been shown that ROS generated by the mitochondrial electron transport chain (ETC) can induce ER stress (27) and sustain ILC3 activation (28). Thus, we investigated potential involvement of mitochondrial ROS in XBP1s expression. Sort-purified mouse siLP ILC3s were stimulated with IL-23 and IL-1β with or without mitochondrial ROS inhibitors, including the mitochondria-targeted antioxidant MitoTEMPO as well as mitochondrial ETC complex I/III inhibitors rotenone and antimycin A. We also tested the impact of tauroursodeoxycholic acid (TUDCA), a chemical chaperone that alleviates global ER stress by improving ER protein folding (17). Cell lysates were analyzed for the expression of *Xbp1s* mRNA by qPCR. Treatment with either MitoTEMPO or rotenone/antimycin A thwarted IL-23/IL-1β-induced *Xbp1* splicing in ILC3s. However, the impact of TUDCA on IL-23/IL-1β-induced *Xbp1s* expression was limited (**Supplemental Figure 4**). These results were confirmed by intracellular staining of XBP1s in ILC3s (**Figure 2G; Supplemental Figure 5**). Furthermore, we exposed mouse siLP ILC3s to hydrogen peroxide for 4 hours to induce ROS (29), resulting in the

upregulation of XBP1s in ILC3s. This induction of XBP1s was reversed by the antioxidant N-acetyl cysteine (NAC) (**Figure 2H**). In contrast, co-treatment with the PERK inhibitor GSK2606414 did not alter the level of XBP1s (30) (**Supplemental Figure 5**). These data demonstrate that IRE1α/XBP1 activation in stimulated ILC3s requires ROS generated by the mitochondrial ETC, a vital event for ILC3 activation (28). It also suggests that the selective IRE1α/XBP1 activation in ILC3s is distinct from the canonical ER stress response, which involves all three UPR branches and is attenuated by chemical chaperones such as TUDCA (11).

IRE1α/XBP1 augments cytokine production in mouse and human ILC3s

Given that ER stress sustains ILC3 cytokine production and that inflammatory stimuli selectively activate IRE1α/XBP1 in ILC3s, we next asked whether the IRE1α/XBP1 pathway is required for ILC3 cytokine production. We crossed *Ire1α*$^{flox/flox}$ with *Rorc-Cre* mice to generate *Ire1α*$^{\Delta Rorc}$ mice. The deletion of exons 16 and 17 of *Ire1α* disrupts its endoribonuclease activity, precluding the formation of *Xbp1s* mRNA (31). All ILC3 subsets (CCR6^{+}, NKp46^{+}, and CCR6^{-} NKp46^{-} [double-negative, DN]) were equally represented in the small intestine and colon of *Ire1α*$^{\Delta Rorc}$ mice and their *Ire1α*$^{flox/flox}$ littermates (**Figure 3A, B**). Similarly, the pool of RORγt^{+} T cells in the small intestine and colon of *Ire1α*$^{\Delta Rorc}$ mice were unchanged at steady state (**Supplemental Figure 6**). However, fewer siLP and colonic ILC3s from *Ire1α*$^{\Delta Rorc}$ mice stimulated *ex vivo* with IL-23 and IL-1β produced IL-22 and IL-17A than did ILC3s from *Ire1α*$^{flox/flox}$ littermates (**Figure 3C, D**). These data indicate that the IRE1α/XBP1 pathway directly contributes to cytokine production in response to inflammatory cytokines in all ILC3 subsets.

Ire1α*$^{\Delta Rorc}$ *mice are vulnerable to intestinal infection due to impaired ILC3s

Since fewer ILC3s from *Ire1α*$^{\Delta Rorc}$ mice produced protective cytokines, we investigated the functional relevance of IRE1α/XBP1 deficiency in ILC3s in models of intestinal infection that cause barrier damage and activate ILC3s. We chose to examine *Ire1α*$^{\Delta Rorc}$ mice in the acute phases of

infection by either *Clostridium difficile* (*C. difficile*) or *Citrobacter rodentium* (*C. rodentium*), since ILC3-derived IL-22 is essential to preserve the epithelial barrier function, while $CD4^+$ T cells are dispensable at this stage (28, 32-35). The small intestine and colon of $Ire1\alpha^{\Delta Rorc}$ mice and control littermates appeared morphologically similar in the absence of infection (**Supplemental Figure 7**). Mice were orally administrated with *C. difficile* after treatment with antibiotics to induce dysbiosis (**Figure 4A**). $Ire1\alpha^{\Delta Rorc}$ mice lost more weight and had higher clinical scores than did their $Ire1\alpha^{flox/flox}$ littermates (**Figure 4B, C**). Consistently, $Ire1\alpha^{\Delta Rorc}$ mice had more severe colitis as indicated by colon length shortening, histology scores, as well as goblet cell loss visualized by alcian blue/PAS staining (**Figure 4D-F**). On day 5 post-infection, fewer colonic ILC3s from $Ire1\alpha^{\Delta Rorc}$ mice produced IL-22 and IL-17A than did ILC3s from $Ire1\alpha^{flox/flox}$ mice (**Figure 4G**). ILC3 cytokines are essential for recruitment of innate immune cells including neutrophils during acute *C. difficile* infection (33). In comparison to $Ire1\alpha^{flox/flox}$ mice, recruitment of neutrophils and inflammatory monocytes was impaired in the colon of $Ire1\alpha^{\Delta Rorc}$ mice (**Figure 4H; Supplemental Figure 8**), as was compromised intestinal barrier integrity gauged by FITC-dextran permeability (**Figure 4I**), and exacerbated bacterial translocation to the liver and mesenteric lymph nodes (mLN) (**Figure 4J**). Moreover, expression of mucins and antimicrobial peptides was diminished in the colonic tissue of $Ire1\alpha^{\Delta Rorc}$ mice with *C. difficile* infection (**Figure 4K**). Since *Rorc-Cre* is expressed not only in ILC3s but also in T lymphocytes, we examined $Ire1\alpha^{\Delta Rorc}Rag^{-/-}$ and $Ire1\alpha^{flox/flox}Rag^{-/-}$ control mice to account for any potential effects on T cells. Upon acute *C. difficile* infection, $Ire1\alpha^{\Delta Rorc}Rag^{-/-}$ mice developed more severe disease as indicated by weight loss, clinical scores, shortening of colon length, histology score, and goblet cell depletion (**Supplemental Figure 9**), recapitulating the phenotype of $Ire1\alpha^{\Delta Rorc}$ mice. In addition, $Ire1\alpha^{\Delta Rorc}$ mice were also more susceptible than $Ire1\alpha^{flox/flox}$ mice to *C. rodentium* infection as assessed by their progressive weight loss, colony-forming unit (CFU) in the feces, shortening of colon length, histology score, goblet cell loss (alcian blue/PAS), and epithelial cell proliferation (Ki67) (**Supplemental Figure 10**) (36-38). Overall, these data demonstrated that impaired production of

ILC3-derived cytokines renders *Ire1α*$^{\Delta rorc}$ mice highly susceptible to acute infection by *C. difficile* or *C. rodentium*.

Ire1α$^{\Delta Rorc}$ *mice are more susceptible to DSS-induced colitis*

To further assess the impact of IRE1α/XBP1 in ILC3 functions *in vivo*, we examined DSS-induced acute colitis, an epithelial injury model of IBD. *Ire1α*$^{\Delta Rorc}$ mice lost more weight and had higher clinical scores than did *Ire1α*$^{flox/flox}$ controls upon DSS challenge (**Figure 5A, B**). Additionally, *Ire1α*$^{\Delta Rorc}$ mice had shorter colons and higher histology score with acute colitis (**Figure 5C, D**). *Ire1α*$^{\Delta Rorc}$ mice with colitis also had extensive goblet cell depletion, reduced epithelial proliferation, and elevated epithelial apoptosis, visualized by staining with alcian blue/PAS, Ki67, and cleaved caspase-3 respectively (**Figure 5E-G**). When challenged with higher dose of DSS in the drinking water, fewer *Ire1α*$^{\Delta Rorc}$ mice survived than did control littermates (**Figure 5H**). These data demonstrate that *Ire1α*$^{\Delta rorc}$ mice are more susceptible to DSS-induced acute colitis. To dissect the potential confounding impact of T cells in the observed phenotype, we repeated the experiment using *Ire1α*$^{\Delta Rorc}$*Rag*$^{-/-}$ and *Ire1α*$^{flox/flox}$*Rag*$^{-/-}$ control mice. *Ire1α*$^{\Delta Rorc}$*Rag*$^{-/-}$ mice developed more severe acute DSS colitis as indicated by weight loss, clinical score, shortening of colon length, histology score, goblet cell loss (alcian blue/PAS), and epithelial cell proliferation (Ki67) (**Supplemental Figure 11**), corroborating the phenotype of *Ire1α*$^{\Delta Rorc}$ mice.

To investigate the mechanisms underpinning susceptibility of *Ire1α*$^{\Delta rorc}$ mice to DSS-induced colitis, we sort-purified colonic ILC3s from *Ire1α*$^{\Delta Rorc}$ and *Ire1α*$^{flox/flox}$ mice with DSS colitis for bulk RNA sequencing. In comparison to control ILC3s, skewed expression of a broad spectrum of genes was evident in *Ire1α*$^{\Delta Rorc}$ ILC3s (**Figure 5I, J and Supplemental Figure 12**). The downregulated transcripts in *Ire1α*$^{\Delta Rorc}$ ILC3s included ER stress response/UPR-associated genes, such as those encoding ER chaperones (*Dnajb9*, *Hspa5*), transcription factors (*Nfkbiz*, *Hes1*, *Creb3l2*), and a neurotrophic factor (*Manf*). mRNAs encoding ribosomal proteins (*Rpl*,

Rps), signal peptidase complex subunits (*Spcs2*, *Spcs3*), Sec61 translocon components (*Sec61b*, *Sec61g*, *Ssr4*), which control mRNA translation and ER protein translocation, also declined in *Ire1α*$^{\Delta Rorc}$ ILC3s. In addition, transcripts for cytokines, including *Il22*, *Il17a*, *Il17f*, and several activation markers, such as *Ccr9*, *Cd69*, *Fos*, *Dusp1*, were diminished in *Ire1α*$^{\Delta Rorc}$ ILC3s. Genes showing heightened expression in *Ire1α*$^{\Delta Rorc}$ ILC3s included *Cxcr5*, which suppresses cytokine secretion of CCR6+ ILC3s (39), various components of the antigen presentation machinery (*Ctse*, *Ctsh*, *Cd74*, *Cd83*), and several involved in pro-apoptotic signaling (*Bclaf3*, *Casp9*). GO enrichment analysis uncovered decreased pathways in *Ire1α*$^{\Delta Rorc}$ ILC3s such as cytoplasmic translation, chemokine production, and lymphocyte activation (**Figure 5K and Supplemental Figure 13**). In conclusion, transcriptomic analysis of colonic ILC3s from *Ire1α*$^{\Delta Rorc}$ mice with DSS-induced colitis corroborates diminished expression of ER stress genes and cytokines, and further indicate the induction of pro-apoptotic genes that can contribute to dysregulated ILC3 functions.

Exogenous IL-22 accelerates recovery from acute DSS colitis in Ire1α*$^{\Delta Rorc}$ *mice

Given the diminished production of IL-22 by *Ire1α*$^{\Delta Rorc}$ ILC3s, we next explored whether exogenous IL-22 could mitigate the susceptibility of *Ire1α*$^{\Delta Rorc}$ mice to DSS-induced colitis. I *Ire1α*$^{\Delta Rorc}$ and *Ire1α*$^{flox/flox}$ mice were subjected to a 7-day regimen of 3.5% DSS to induce acute colitis, followed by a recovery period from day 7 to 11 without DSS treatment. During this recovery phase, one group of mice received daily intraperitoneal injections of mouse recombinant IL-22, while another group received vehicle only. The *Ire1α*$^{\Delta Rorc}$ mice exhibited less recovery compared to *Ire1α*$^{flox/flox}$ mice. However, treatment with IL-22 significantly improved recovery in *Ire1α*$^{\Delta Rorc}$ mice, as evidenced by changes in weight, clinical scores, colon length, histology scores, and goblet cell numbers (**Figure 6A-E**). In contrast, administration of IL-22 had less impact on the recovery of *Ire1α*$^{flox/flox}$ mice with normal ILC3s. These findings highlight the critical role of IL-22 deficiency in the heightened susceptibility of *Ire1α*$^{\Delta Rorc}$ mice to intestinal inflammation.

Ire1α$^{\Delta Rorc}$Rag$^{-/-}$ mice develop exacerbated colitis upon adoptive T-cell transfer

To explore the involvement of IRE1α/XBP1 in intestinal ILC3s beyond acute colitis models, we conducted a T-cell transfer-induced colitis, which represents a chronic immune-mediated model of IBD (40, 41). CD4^{+}CD45RB^{high} T cells were sort-purified from wild-type C57BL/6 mice and transferred into *Ire1α$^{\Delta Rorc}$Rag$^{-/-}$* and *Ire1α$^{flox/flox}$Rag$^{-/-}$* (control) littermates. After adoptive transfer, *Ire1α$^{\Delta Rorc}$Rag$^{-/-}$* mice developed more severe colitis, as indicated by progressive weight loss, clinical scores, colon length, and histological changes up to day 45 post-transfer (**Figure 6F-J**). In addition to inflammation, *Ire1α$^{\Delta Rorc}$Rag$^{-/-}$* mice showed more severe goblet cell depletion and fibrosis by alcian blue/PAS and Masson's trichrome staining, respectively (**Figure 6I, J**). These data indicate that IRE1α/XBP1 in ILC3s is protective against chronic, immunological colitis in mice, which further supports its clinical relevance in human IBD.

IRE1 modulators control production of IL-22 in human intestinal ILC3s

Considering the crucial function of IRE1α in mouse ILC3s, we examined the expression of IRE1α (encoded by *ERN1* in human) and other ER stress genes in human intestinal ILC3s during IBD. We reanalyzed the scRNA-seq data of colonic LP cells from healthy individuals and UC patients in a published database (42). Colonic ILC3s from both inflamed and non-inflamed ulcerative colitis (UC) mucosa showed increased expression of *ERN1* compared to those from healthy controls (**Figure 7A**). Additionally, the expression of *ATF4*, *SSR1*, and *DNAJB9*, which are transactivated by XBP1s (43-45), was elevated in both inflamed and non-inflamed UC tissues. In contrast, *PDIA6*, *HSPA5*, *HERPUD1*, and *DDIT4* exhibited minimal changes or were downregulated in UC tissues (**Figure 7B**). These findings are consistent with our observation that inflammation specifically activates the IRE1α/XBP1 branch of the UPR in ILC3s.

Since IRE1α/XBP1 enhances mouse ILC3 activation, we next asked whether this pathway also impacts the function of human intestinal ILC3s. We recruited adult patients without a history

of digestive disease who were undergoing colonoscopy for colon cancer screening. Colonic biopsies were collected, ILC3s were FACS sorted and stimulated *ex vivo* with IL-23, with or without IRE1 modulators; these included selective IRE1 inhibitors 4μ8C and KIRA6 (46, 47) and a selective IRE1 activator IXA4 (48). Co-treatment with 10 ng/mL IL-23 and either 4μ8C or KIRA6 reduced the frequencies of XBP1s$^+$ and IL-22-producing ILC3s by >60% (**Figure 7C, D**). Conversely, IXA4 enhanced the frequencies of XBP1s$^+$ and IL-22-producing ILC3s induced by a low concentration of IL-23 (0.1 ng/mL) (**Figure 7E, F**). We conclude that IRE1α/XBP1 positively regulates the production of IL-22 in human intestinal ILC3s.

Intestinal XBP1s$^+$ ILC3s in CD patients predict response to ustekinumab

Given that the IRE1α/XBP1 pathway augments cytokine production in response to IL-23 by human ILC3s and that IL-23 blockers have been proven effective in CD, we investigated whether the level of pre-treatment XBP1s in ILC3s correlates with response of CD patients to the non-selective anti-IL-23 antibody ustekinumab. We recruited patients with active CD, which were defined as Simple Endoscopic Score for CD (SES-CD) segment score ≥3. Biopsies were collected from inflamed intestinal mucosa (n = 28) within three months before they started ustekinumab and cryopreserved for batch processing as we previously described (49). Patients' responses were assessed clinically and/or endoscopically 8-40 weeks after the initiation of ustekinumab. Elevated frequencies of XBP1s$^+$ ILC3s in intestinal mucosa positively correlated with response to ustekinumab (**Figure 7G**). These data suggest that the activity of pre-treatment IRE1α/XBP1 in intestinal ILC3s predicts the response to ustekinumab.

Discussion

This study reveals that inflammation in the gastrointestinal tract triggers the IRE1α/XBP1 pathway in ILC3s. In mice, this pathway was crucial for optimal production of IL-22 and IL-17 by ILC3s, leading to resistance against acute infections caused by *C. difficile* or *C. rodentium*, acute

colitis induced by DSS, and chronic colitis induced by T-cell transfer. In humans, activation of IRE1α/XBP1 amplified IL-22 production by intestinal ILC3s in response to IL-23. A specific activator of IRE1 enhanced IL-22 production by colonic ILC3s when exposed to low concentrations of IL-23, while inhibitors of IRE1 dampened IL-22 production in response to IL-23. The ER stress response triggered by inflammation in ILC3s exhibited a non-canonical pattern. Specifically, it selectively engaged the IRE1α/XBP1 pathway without activating the other two UPR branches (**Supplemental Figure 14**). Consequently, TUDCA, a chemical chaperone known to suppress canonical ER stress in various cell types and organs (17, 27, 50), did not significantly affect XBP1s induced by inflammatory cytokines. Furthermore, this response relied on mitochondrial ROS. As evidence, a brief exposure to low-dose H_2O_2 directly stimulated IRE1α/XBP1, while mitochondria-targeted antioxidants and ETC inhibitors decreased XBP1s expression in ILC3s. A previous study showed that ROS enhance ILC3 cytokine production and their ability to defend against *C. rodentium* infection (28). Our latest findings further this research, suggesting that activation of IRE1α/XBP1 is at least one of the mechanisms through which ROS stimulate ILC3s. The selective activation of IRE1α/XBP1 by ROS in ILC3s is not unprecedented; in fact, ROS-induced XBP1 activation was also observed in macrophages stimulated through Toll-like receptors (51). Whether this pathway is generalizable to other immune cell types is currently unknown.

It is worth noting that ILC3s displayed strong rhythmic expression of *Xbp1s*, reaching its peak at ZT12 and aligning with the expression patterns of *Il22* and the clock gene *Per1*. This finding supports the idea that ILC3 functions, similar to many other functions of the gastrointestinal system, are synchronized with the circadian rhythm. Circadian oscillation of the IRE1α/XBP1 pathway was also observed in the liver and shown to modulate lipid metabolism (52). Enteric neurons are localized adjacent to ILC3s in the gut and secrete neuropeptide VIP upon feeding. VIP induces rhythmic expression of IL-22 via VIPR2 on intestinal ILC3s, although the intracellular pathway downstream of VIPR2 remains unclear (24-26). We discovered that a brief exposure to

VIP or a VIPR2 agonist prompted the activation of XBP1s in ILC3s. This suggests that the IRE1α/XBP1 pathway may partly underlie VIP's regulation of rhythmic ILC3 function in the gut. Interestingly, the expression of *Chop* peaked at ZT0 when *Xbp1s*, *Il22*, and *Per1* transcripts were at their nadir. CHOP is transcription factor mainly activated by the PERK-eIF2α branch of the UPR (11). It has a pro-apoptotic function during prolonged ER stress, but can also repress T-bet (53), which promotes the conversion of IL-22-producing ILC3s into IFNγ-producing ILC1s in mice (54, 55). Future studies are needed to explore whether CHOP regulates the rhythmicity and plasticity of ILC3s.

Here, we demonstrate that IRE1α/XBP1 strengthens IL-23 signaling in ILC3s, enhancing protection against both acute and chronic colitis in mice. This finding is somewhat unexpected, given that dysregulated IL-23 is known to be pathogenic in human IBD. One potential explanation for this apparent paradox is that IRE1α/XBP1-enhanced IL-23 signaling may be beneficial in ILC3s by stimulating the expression of IL-22, which improves epithelial integrity and impedes bacterial translocation. Conversely, it may be detrimental in other cell types, including Th17, Th1-like, IL-17-expressing cytotoxic T cells (Tc17), γδ T cells, and NKT cells, where IL-23 promotes the production of proinflammatory cytokines such as TNF-α, IFN-γ, and IL-6 (56) (**Supplemental Figure 14**). Another potential explanation is that IL-23 activates multiple downstream pathways in addition to IRE1α/XBP1, such as the Janus kinases (JAKs)-STAT pathways, which are important drug targets in IBD. While the IL-23-IRE1α/XBP1 pathway in ILC3s may be protective in colitis, other IL-23 targets including JAK2 and TYK2 are pathogenic (57). This may explain why the loss of IRE1α/XBP1 in ILC3s exacerbates colitis in mice, while suppressing IL-23 globally benefits a subset of patients with IBD.

Therapies targeting IL-23, such as ustekinumab and risankizumab, have emerged as crucial strategies in managing IBD. However, over half of IBD patients do not respond to IL-23 antagonists, and currently available biomarkers fail to predict their responses. Notably, levels of IL-23 in peripheral blood or intestinal mucosa have proven ineffective in predicting response to

anti-IL-23 therapies. Our research uncovered that elevated frequencies of pre-treatment XBP1s$^+$ ILC3s were associated with a more favorable response to ustekinumab. This suggests that XBP1s$^+$ ILC3s may indicate increased sensitivity to IL-23 in IBD patients, making them suitable candidates for biological therapies that diminish IL-23 availability. This finding aligns with previous observations showing that CD patients with higher baseline levels of IL-22 were more likely to benefit from brazikumab, another IL-23 antagonist (58). Another explanation could be that high levels of XBP1s$^+$ ILC3s and IL-22 reflect an enhanced capacity of patients to maintain ILC3-mediated protective mechanisms alongside the inhibition of pathogenic T cells (**Supplemental Figure 14**). Ongoing studies aim to validate the predictive value of XBP1s$^+$ ILC3s in larger, independent cohorts of IBD patients starting ustekinumab or newer selective anti-IL-23 antibodies including risankizumab and mirikizumab.

Methods

Sex as a biological variant

We included both male and female sexes in mouse and human studies. Sex was not considered as a biological variable in the studies.

Mice

Ire1α$^{flox/flox}$ mice were a generous gift from R. Kaufman (31). *Rorc-Cre* mice were generated by Gerard Eberle *et al*.(59) and provided by A. Tumanov (University of Texas Health Science Center at San Antonio). *Rag$^{-/-}$* mice were purchased from the Jackson Laboratory. All mice used for experiments were on a C57BL/6 background and 8-12 weeks of age at the time of experiment. Mice were housed in regular filter-top cages with free access to sterile water and food in a pathogen-free barrier facility fully staffed and equipped by the Washington University Division of Comparative Medicine with daily monitoring by highly trained staff. Environmental conditions are reproducibly regulated for temperature, humidity, lighting, caging, bedding, and water. The

room housing animals is maintained at humidity 30-70%, temperature 20-26°C (68-79°F) with ventilation sufficient to maintain appropriate temperature and humidity ranges and to control odor. A light:dark cycle of 12 hours on:12 hours is maintained in the animal facility. Practices are followed for consistent husbandry and animal line maintenance per IACUC protocols. E.g., we use genotypes from the same litter to control for litter effects. We use single pairs for continuous breeding, and refresh breeders at ~8 months for a female and ~1 year for a male. To avoid crowding, we keep 5 post-weaning mice per cage, 3 adults and 1 litter only up to 14 days old, or 2 dams with 2 young litters only <7 days of age per protocol. Both male and female mice were used in the experiments. To avoiding phenotypic variability, co-housed, sex- and age- matched littermates were randomly assigned to treatment and control groups. Each treatment group were compared with a control group studied in parallel. 8-week-old, wild-type C57BL/6 mice for circadian rhythm study were purchased from Jackson Laboratory and housed in light-controlled cabinets as previously described (2). All studies were conducted in accordance with the Washington University Animal Studies Committee. We have implemented several crucial strategies to mitigate variability in gut microbiome composition within our colitis models (33, 60, 61). First, we adopted the practice of cohorting mice from birth to minimize cage effects, and we ensured the randomization of littermate mice across experimental groups to ensure an equitable distribution of potential sources of variability. As mentioned above, we maintained standardized housing conditions, including elements such as temperature, humidity, and light cycles, to establish a stable and highly controlled environment. Furthermore, we have used a uniform diet for all mice to control dietary influences on the gut microbiome, thereby minimizing fluctuations in microbial composition. These comprehensive measures have collectively contributed to the creation of a more controlled experimental framework in our colitis research.

Tissue preparation and single cell isolation from mice

Small intestinal and colonic LP cells were isolated as we previously described (2, 33, 62). Briefly, mouse intestines were dissected out and washed with ice-cold HBSS/HEPES. Mesenteric fat and Peyers' patches were removed and intestines were cut open longitudinally. Intestines were incubated in HBSS-EDTA to remove intestinal epithelium. Intestines were washed, cut into small pieces, and shaken in complete RPMI with collagenase IV at 37°C for digestion (30 minutes for small intestine, 45 minutes for colon). The digestant was then filtered through a 100μm strainer and washed with ice-cold HBSS/HEPES. Lamina propria cells further purified through a 40/70 Percoll density gradient.

Patient recruitment

Adult patients with active Crohn's disease (Simple Endoscopic Score for CD [SES-CD] segment score ≥3) who were about to start ustekinumab were recruited for study. Mucosal samples were collected within 3 months before the initiation of ustekinumab. 6 endoscopic biopsies are taken from inflamed mucosa during routine colonoscopy. Specimens from inflamed intestinal mucosa were identified intraoperatively by the endoscopist and subsequently confirmed by a blinded GI pathologist. Samples were cryopreserved within 20-30 min of collection as we described (49). Briefly, the biopsies were kept in complete RPMI medium on ice immediately after collection and transported to the lab, where they were changed into a freezing medium (10% dimethyl sulfoxide in fetal calf serum), transferred to a pre-chilled Mr. Frosty™ (ThermoFisher) container with isopropanol frozen and kept in -80°C. The samples were then transferred to liquid nitrogen 24h later for storage.

Patients' responses were assessed clinically and/or endoscopically 8-40 weeks after the initiation of treatment. Clinical response was defined as a decrease in Harvey-Bradshaw Index (HBI) ≥3, a decrease in Crohn's Disease Activity Index (CDAI) ≥100 points from baseline, or CDAI <150. Endoscopic response was defined as a ≥50% reduction in SES-CD.

Preparation of single-cell suspension from endoscopic biopsies

Frozen specimens were processed in batches to minimize variation as we described(49). Briefly, samples were thawed in 37°C water bath, rinsed with ice-cold PBS, and digested in complete RPMI medium containing 100 mg/mL of Liberase TH and 100 mg/mL of DNase I at 37°C for 30 min under agitation. Cell suspension is then filtered through a 40 μm cell strainer and washed twice with cold PBS for further analysis.

C. difficile colitis

C. difficile infection of mice was performed as we previously described (33). Briefly, 8-10-week age- and gender-matched littermates were pretreated with antibiotic mixture (0.4 mg/mL kanamycin, 0.035 mg/mL gentamicin, 0.035 mg/mL colistin, 0.215 mg/mL metronidazole, and 0.045 mg/mL vancomycin; all from Sigma-Aldrich) added to drinking water for 4 days. Next, mice received clindamycin (10 mg/kg, i.p.; Sigma-Aldrich). After 1 day, mice were infected with 10^8 CFU of *C. difficile* (VPI 10463 strain) by gavage. Mice were weighed and monitored daily during the entire protocol with a clinical severity score from 0 (normal) to 15 (33). Mice were sacrificed on day 5 of infection and colons were collected for histology and IHC. Samples were analyzed blindly using histological scores as previously described (33).

Translocation of C. difficile

Spleen, liver, and mesenteric lymph nodes were harvested on day 2 of *C. difficile* infection. Bacterial 16S rDNA were extracted using the PureLink Microbiome DNA Purification kit (ThermoFisher Scientific) and quantified by qPCR using primers complementary to Eubacteria 16S rDNA conserved region. The bacterial load was determined by a standard curve with serial dilutions of *E. coli* genomic DNA, and the CFU per gram of tissue was determined by dividing gene levels by sample weight as we previously described (33).

Measurement of intestinal permeability with FITC-dextran

On day 3 of *C. difficile* infection, mice received 200 μL FITC-dextran (70,000 D; Sigma-Aldrich) suspension (250 mg/kg) by gavage. After 4 h, mice were anesthetized, blood was collected by caudal puncture, and fluorescence readings were performed in a Multi-Mode Microplate Reader (Synergy HT) at 485/528 nm (excitation/emission). A standard curve was prepared with serial dilutions of FITC-dextran in PBS (33).

C. rodentium infection

8-10-week age- and gender-matched littermates were orally administered 2×10^9 *C. rodentium*, strain DBS100 (ATCC), as we previously described (28, 63). Body weight of mice was measured daily until day 10 or 20, when the mice were sacrificed for tissue collection. Samples were analyzed blindly using histology scores based on inflammation, edema, epithelial defects, crypt atrophy, and hyperplasia on a scale from 0 to 4 (64).

DSS-induced colitis

For acute colitis, mice received 3.5-4% (w/v) DSS (MW 36,000–50,000; MP Biomedicals) in drinking water for 7-8 days. Body weight and clinical scores were measured daily as previously described (17). For administration of IL-22, mice were injected intraperitoneally with 1 μg recombinant mouse IL-22 daily.

Adoptive T-cell transfer-induced colitis

Splenic CD4+CD45RB^{high} T cells were sort-purified from WT mice. 5 x 10^5 T cells were transferred intraperitoneally into co-housed *Ire1α*$^{\Delta Rorc}$*Rag*$^{-/-}$ and *Ire1α*$^{flox/flox}$*Rag*$^{-/-}$ mice. The mice were weighed every 5 days post-transfer. Clinical score was graded on a scale of 0-5 based on decreased activity, hunched posture, ruffled fur, rate of breathing, shrunken eyes, shivering, rectal

bleeding, and diarrhea as previously described (65, 66). The mice were euthanized on day 45 post-transfer and the colons were collected for measurement of length and histology.

Flow cytometry

The following antibodies were used for flow cytometry of mouse cells: CD3e (145-2C11, BioLegend), CD4 (RM4-5, BioLegend), CD5 (53-7.2, BioLegend), CD11b (M1/70, BioLegend), CD11c (N41B, ThermoFisher), CD19 (6D5, BioLegend), CD45 (30-F11, BioLegend), CD90.2 (53-2.1, BioLegend), CCR6 (140706, BD Biosciences), B220 (RA3-6B2, BioLegend), Gr-1 (RB6-8C5, BioLegend), KLRG1 (2F1, BioLegend), NK1.1 (PK136, BioLegend), NKp46 (29A1.4, BioLegend), TER-119 (TER-119, BioLegend), RORγt (AFKJS-9, ThermoFisher), FoxP3 (MF-14, BioLegend), GATA3 (L50-823, BD Biosciences), T-bet (eBio4B10, ThermoFisher), Eomes (Dan11mag, ThermoFisher), IL-22 (1H8PWSR, ThermoFisher), IL-17A (TC11-18H10, BD Biosciences), XBP1s (Q3-695, BD Biosciences). The following antibodies were used for flow cytometry of human cells: CD3 (UCHT1, BioLegend), CD5 (UCHT2, Biolegend), CD11b (ICRF44, BioLegend), CD11c (Bu15, BioLegend), CD14 (QA18A22, BioLegend), CD19 (HIB19, BioLegend), CD45 (2D1, BioLegend), CD117 (104D2, BioLegend), CD127 (A019D5, BioLegend), NKp44 (P44-8, BioLegend), FcεRIα (AER-37, BioLegend), RORγt (REA278, Miltenyi), IL-22 (2G12A41, BioLegend). Stained single-cell suspensions were analyzed on a FACSCanto II or a FACSymphony A3 cytometer (BD Biosciences). BD FACS ARIA II (BD Biosciences) was used for cell sorting. Analysis was performed using BD FACS Diva Software v 8.0.1 and FlowJo v10 (FlowJo LLC).

Generation and analysis of bulk RNA-seq data

Colonic LP cells were isolated from the colons of *Ire1α*$^{\Delta Rorc}$ (KO) and *Ire1α*$^{flox/flox}$ (CTR) mice with acute DSS colitis. More than 5,000 ILC3s per mouse were sorted into RLT lysis buffer (provided in QIAGEN RNeasy Plus Micro Kit). Total RNA was extracted by QIAGEN RNeasy Plus

Micro Kit. RNA integrity number (RIN) was determined using Agilent Bioanalyzer. RIN for all samples were greater than 9. The following steps were described in Peng and Cao et al. (62). In short, cDNA was prepared using SMARTer Ultra Low RNA kit for Illumina Sequencing (Takara-Clontech) at the Genome Technology Access Center (GTAC) at Washington University. cDNA was then fragmented and blunt ended. A base was added to 3′ ends of cDNA fragments, and Illumina sequencing adapters were ligated to the ends. Ligated fragments were then amplified and sequenced (Illumina HiSeq). After basecalling and demultiplexing, RNA-seq reads were aligned to mm10 genome. Aligned gene counts were processed using DESeq2 package (67) with R (version 4.3.2). Genes with fewer than 10 counts among all samples were excluded. For DEG analysis, only protein-coding genes with an average expression of > 100 counts per sample were used. The threshold of DEG was set as "adjusted p value" < 0.05 and |log2FoldChange| > 1. GSEA analysis was performed using clusterProfiler package (68) with R. Genes for GSEA analysis were filtered as protein-coding genes with an average expression > 100 counts and "adjusted p value" < 0.1.

Analysis of scRNA-seq data

The count matrices and cell-barcode associated metadata was downloaded from Smillie et al(42). The cells annotated as "ILCs" were subsetted and processed separately using the Seurat R package. Specifically, only cells with UMI counts between 200 and 3000 were kept, and cells whose percentage of mitochondrial genes were higher than 25% were discarded from the analysis. The resulting "ILCs" dataset was then normalized and scaled using the "Sctransform" algorithm with regression of percentage of mitochondrial genes. Standard PCA and UMAP were run using 20 dimensions. Following this procedure, a DeSeq2-type analysis was performed to obtain the average expression of each gene in the "ILCs" cluster in each patient, for which purpose samples were first "pseudobulked". Specifically, the resulting Seurat object was transformed into a SingleCellExperiment R object after running the function "DietSeurat" followed by

"as.SingleCellExperiment", and matrix of log-transformed counts was generated by running the function "aggregate.Matrix" using the following parameters: groupings were defined by the author-determined metadata slots "sample" and "health", which contained information about the sample ID and the health status of the patient who donated the sample, and the function was set to "sum". Finally, an individual value for the log-transformed expression of *ERN1* was obtained by computing the average between all biopsy sites taken from the lamina propria of each patient identified with a unique patient ID. Represented are X healthy control samples, Y inflamed samples, and Z non-inflamed samples.

Statistics

2-tailed Student t test or one-way ANOVA with Tukey's multiple comparisons test in GraphPad Prism 10.0 (GraphPad software, La Jolla, CA) was used for statistical analysis. P value < 0.05 was considered statistically significant.

Study approval

All human studies were conducted under the approval of the Institutional Review Boards (IRB) of Washington University. Studies were conducted in accordance with the International Conference on Harmonization Good Clinical Practice Guideline, applicable regulations, and the Declaration of Helsinki. Patients provided written informed consent before enrollment. All animal studies were conducted under the approval of the Institutional Animal Care and Use Committee (IACUC) of Washington University.

Data availability

The RNA-seq data were deposited into GEO (accession number: GSE261091). All other data are reported in the Supporting Data Value file.

Author Contributions:

SC conceptualized the study and designed experiments. SC, JLF, KM, QW, ZC performed mouse experiments and data analysis. SC, MCiorba, and PD were responsible for collection of human samples. SC and AUA analyzed human data. RJK provided reagents. SC and MColonna wrote the original draft of the manuscript. All authors reviewed and edited the manuscript. MColonna and SC acquired funding. MColonna supervised the study.

Acknowledgements

We would like to thank Darren Billy Nix, Donald Jones, and Lulu Huang at Washington University Inflammatory Bowel Disease Center for help with IRB, recruitment of patients, and sample collection. We thank Drs. Rodney Newberry, Nicholas Davidson, and all members of the Colonna Laboratory for inspiring discussions. We thank Susan Gilfillan and Marina Cella for helpful comments. Siyan Cao was supported by the Crohn's and Colitis Foundation, American Gastroenterological Association, Lawrence C. Pakula, MD IBD Education & Innovation Fund, Doris Duke Foundation, Washington University Institute of Clinical and Translational Sciences and Digestive Disease Research Core Center, and a NIDDK K08 (1K08DK140612). Matthew Ciorba was supported by Givin' It All For Guts Foundation. Marco Colonna was supported by the Rainin Foundation and by NIH grants R01 DK126969 and R01 DK132327.

Figures

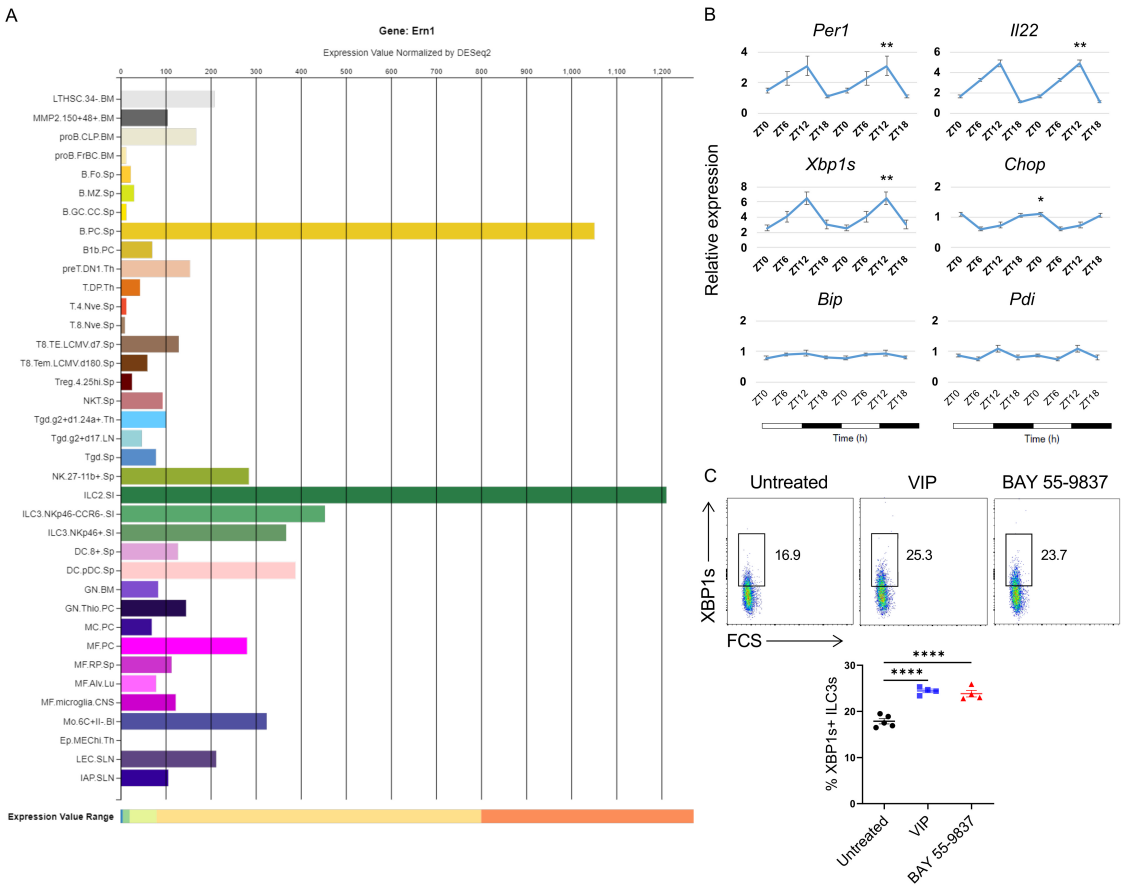

Figure 1. Intestinal ILC3s exhibit high *Ire1α* (*Ern1*) expression and circadian oscillation of *Xbp1s*. (A) Mouse intestinal ILC3s express high level of *Ire1α* (*Ern1*). Expression of *Ern1* in mouse immune cells from http://rstats.immgen.org/Skyline/skyline.html. (B) Gene expression in sorted mouse siLP ILC3s (all subsets included) over a 24h period by qPCR, relative expression to *β-actin*. Statistical analysis was performed using MetaCycle indicated by PJTK_CYCLE value. N=8 per time point. (C) Sorted mouse siLP ILC3s were treated with VIP and BAY 55-9837 (both were 1 μM) for 4 hours, intracellular XBP1s was measured by flow cytometry. P values were calculated using 2-tailed Student t test or one-way ANOVA with Tukey's multiple comparisons test. Error bars indicate SEM. *p<0.05, **p<0.01, ****p<0.0001.

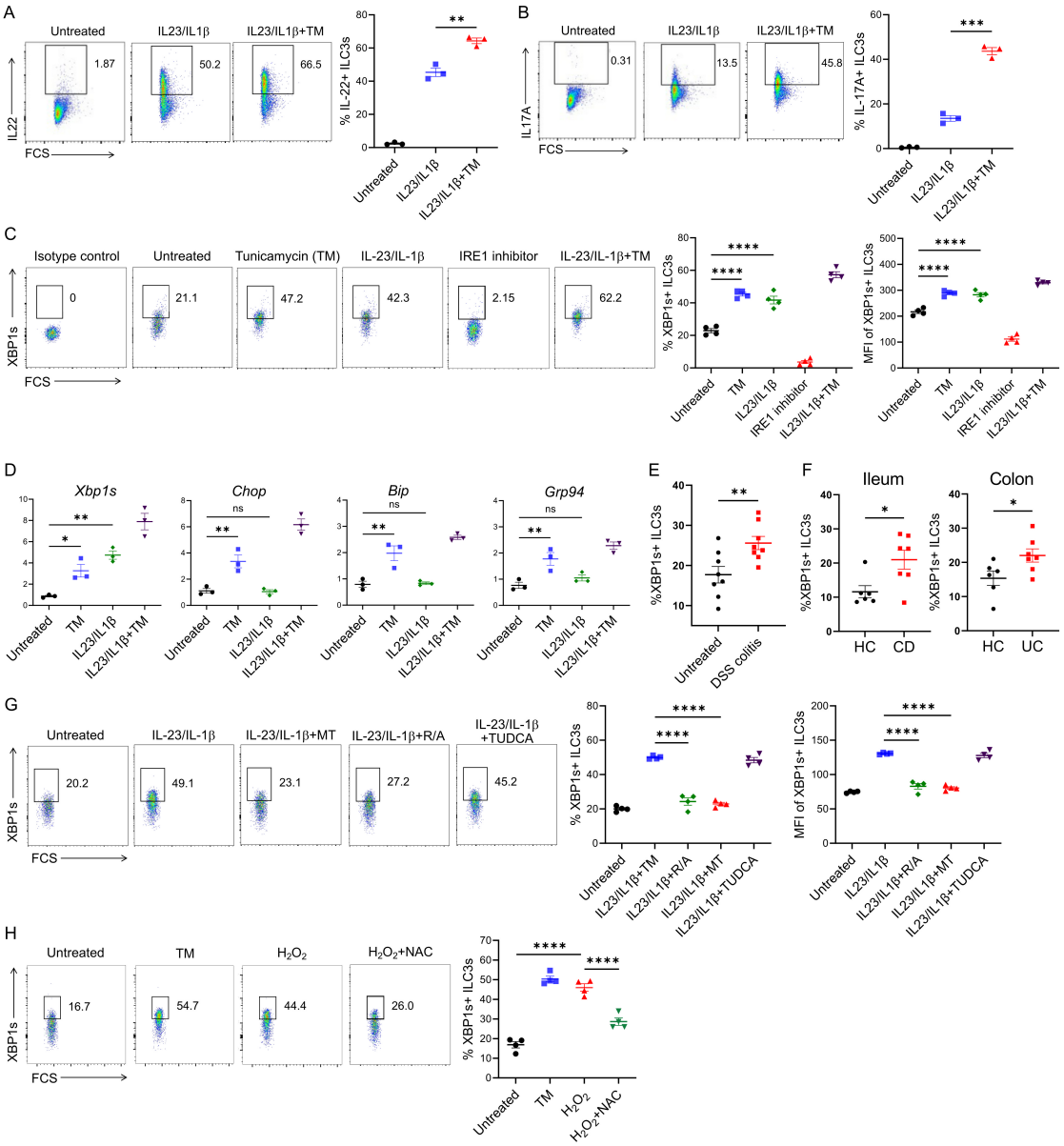

Figure 2. Inflammation and IBD activate IRE1α-XBP1 in ILC3s, which requires mitochondrial ROS. (A and B) Sorted mouse small intestinal lamina propria (siLP) ILC3s (all subsets included) were untreated or treated with 1 ng/mL IL-23, 1 ng/mL IL-1β, 5 υg/mL tunicamycin (TM) for 4 hours (GolgiPlug for the last 3 hours); intracellular cytokines were assessed by flow cytometry. (C and D) Sorted mouse siLP ILC3s (all subsets included) were treated or not as noted with 1 ng/mL IL-23, 1 ng/mL IL-1β, 5 μg/mL tunicamycin (TM), 10 μM IRE1

inhibitor 4μ8C for 4 hours. (C) Intracellular XBP1s was measured by flow cytometry. (D) Expression of UPR components were measured by qPCR relative to *β-actin* (n = 3). (E) Wild-type C57BL/6J mice were either untreated or given 3% dextran sodium sulfate (DSS) in drinking water for 5 days to induce acute colitis, and colonic LP ILC3s were isolated for flow cytometry. The percentage of XBP1s+ colonic LP ILC3s from each mouse is shown (n = 8). (F) Inflamed ileal (for CD) or colonic (for UC) samples and ileal/colonic tissue from healthy controls (HC) were collected for isolation of lymphocytes. Human ILC3s were identified as live $CD45^+Lin^-CD127^+NKp44^+$ lymphocytes. Intracellular XBP1s in ILC3s was detected by flow cytometry. The percentages of XBP1s+ ILC3s in samples from HC, CD and UC patients are shown in the panels. (G) Sorted mouse siLP ILC3s were untreated or treated as noted with 10 ng/mL IL-23, 1 ng/mL IL-1β, 50 μM MitoTEMPO (MT), 0.1 μM rotenone plus 1 μM antimycin A (R/A), or 5 mM tauroursodeoxycholic acid (TUDCA) for 6 hours. (H) Mouse siLP ILC3s were treated with 5 μg/mL tunicamycin (TM), 20 μM hydrogen peroxide (H_2O_2) with or without 5 mM N-acetyl cysteine (NAC) for 4 hours. XBP1s was measured by intracellular staining. Representative plots are shown. Data of all panels represent at least 2 independent experiments. P values were calculated using 2-tailed Student t test or one-way ANOVA with Tukey's multiple comparisons test. Error bars indicate SEM. *p<0.05, **p<0.01, ***p<0.001, ****p<0.0001.

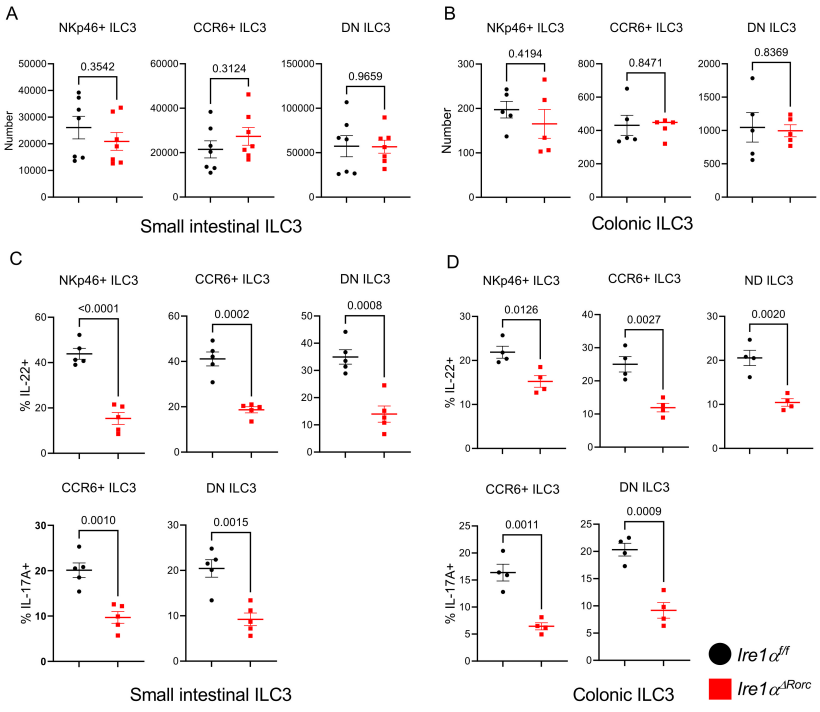

Figure 3. ER stress and IRE1α-XBP1 control cytokine production in ILC3s. Mouse ILC3s were identified as live $CD45^{int}Lin^{-}CD90.2^{hi}$ lymphocytes, which were $NKp46^{+}$, $CCR6^{+}$, or $NKp46^{-}$ $CCR6^{-}$ (double-negative [DN]). ILC3 cell counts in *Ire1α*$^{\Delta Rorc}$ and *Ire1α*$^{flox/flox}$ small intestinal (si) LP (A) and colonic LP (B). siLP cells (C) and colonic LP cells (D) were treated with 1 ng/mL IL-23, 1 ng/mL IL-1β for 4 hours (GolgiPlug for the last 3 hours) and intracellular IL-17A and IL-22 were measured in $CCR6^{+}$, $NKp46^{+}$, and DN ILC3 subsets by flow cytometry (n = 4-5). Data represented at least 3 independent experiments each involving 4-7 mice per group. P values were calculated using unpaired Student's t-tailed). Error bars indicate SEM.

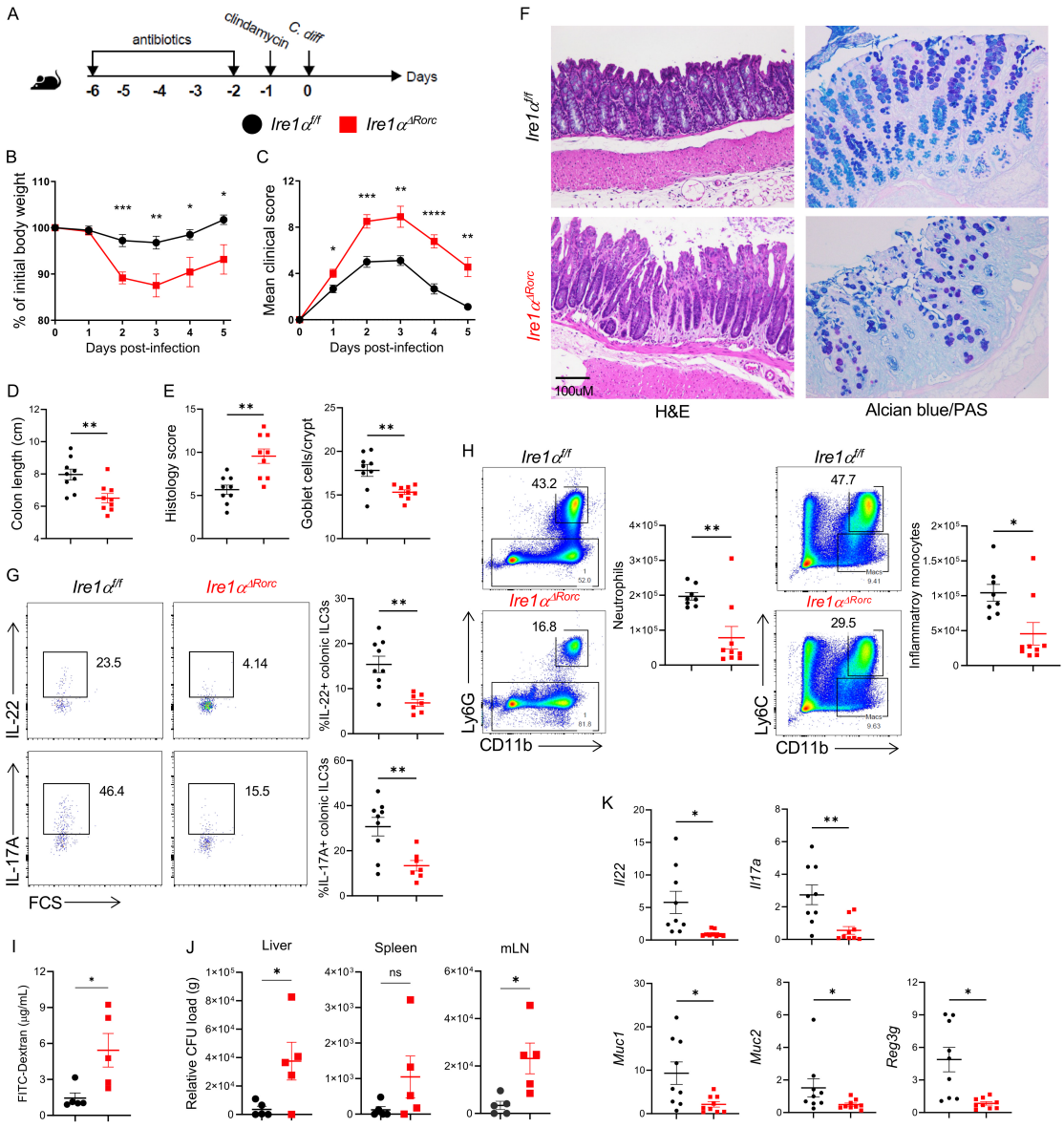

Figure 4: *Ire1α*$^{\Delta Rorc}$ mice are highly susceptible to *C. difficile* infection. (A) *Ire1α*$^{\Delta Rorc}$ and *Ire1α*$^{flox/flox}$ mice were orally infected by *C. difficile* following treatment with antibiotics. (B) Weight loss and (C) clinical scores were measured daily (n = 9-10). (D-F) Mice were sacrificed on day 5 post-infection and colons harvested for measurement of length (D), as well as histology score and goblet cells numbers based on H&E staining and alcian blue/PAS staining (E, F). (G) Colonic LP ILC3s were isolated on day 5 post-infection and stimulated *ex vivo* with 10 ng/mL IL-23, 10 ng/mL IL-1β for 4 hours (GolgiPlug for the last 3 hours); intracellular cytokines were measured by flow

cytometry (n = 7-9). Representative plots are on the left and the percentage of cytokine+ ILC3s in each mouse shown on the right. (H) Representative plots and absolute number of neutrophils and inflammatory monocytes in the colonic lamina propria of *C. difficile*-infected mice on day 2 post-infection (n = 8-9). (I) Mice received FITC-dextran by gavage on day 3 post-infection, serum was collected 4 hours later and FITC-dextran quantitated (n = 5). (J) Bacterial translocation into the liver, spleen, and mesenteric lymph nodes (mLN) was assessed by qPCR on day 3 post-infection (n = 5). (K) Expression of cytokines, mucins, and antimicrobial peptides in the proximal colon on day 5 post-infection was measured by qPCR relative to *β-actin* (n = 7-9). Data represent at least 2 independent experiments, each involving 5-9 mice per group. P values were calculated using unpaired Student's t-test (2-tailed). Error bars indicate SEM. *p<0.05, **p<0.01, ***p<0.001, ****p<0.0001.

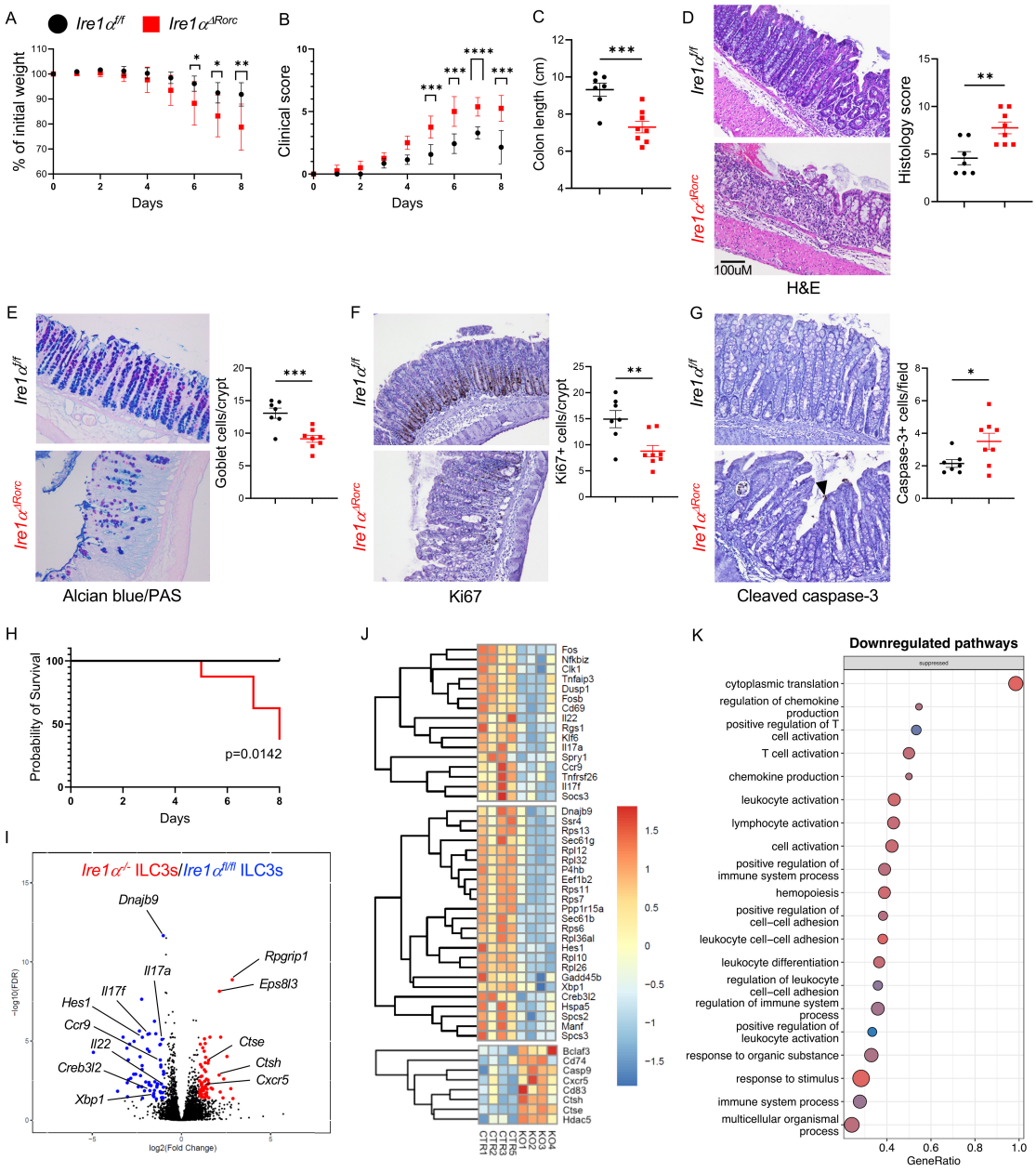

Figure 5: *Ire1α*$^{\Delta Rorc}$ mice are more susceptible to DSS-induced colitis. (A-E) *Ire1α*$^{\Delta Rorc}$ and *Ire1α*$^{flox/flox}$ mice were given 3.5% DSS in drinking water for 7 days followed by one day of fresh untreated water. (A) Weight loss and (B) clinical scores were measured daily (n = 7 or 8). Mice were sacrificed on day 8 of colitis and colons harvested. We measured the following parameters: colon length (C); histology score determined by H&E staining (D); goblet cell numbers assessed

via alcian blue/periodic acid Schiff (PAS) staining (E); and proliferating and apoptotic cells identified through IHC staining for Ki67 (F) and cleaved caspase-3 (G), respectively. (H) *Ire1α*$^{\Delta Rorc}$ and *Ire1α*$^{flox/flox}$ mice were given 4% DSS in drinking water for 8 days and mortality was assessed (n = 7 or 8). Data represent at least 2 independent experiments. (I-K) Bulk RNA sequencing of colonic ILC3s from *Ire1α*$^{\Delta Rorc}$ and *Ire1α*$^{flox/flox}$ mice with DSS colitis (n = 4). (I) Volcano plot of genes with >1.5-fold differential expression in *Ire1α*$^{flox/flox}$ versus *Ire1α*$^{\Delta Rorc}$ ILC3s (blue) and >1.5-fold differential expression in *Ire1α*$^{\Delta Rorc}$ versus *Ire1α*$^{flox/flox}$ ILC3s (red). (J) Heatmap shows selected target genes that were differentially expressed in *Ire1α*$^{\Delta Rorc}$ ILC3s. (K) Downregulated pathways in *Ire1α*$^{\Delta Rorc}$ ILC3s by GO enrichment analysis. P values were calculated using unpaired Student's t-test (2-tailed). Error bars indicate SEM. *p<0.05, **p<0.01, ***p<0.001, ****p<0.0001.

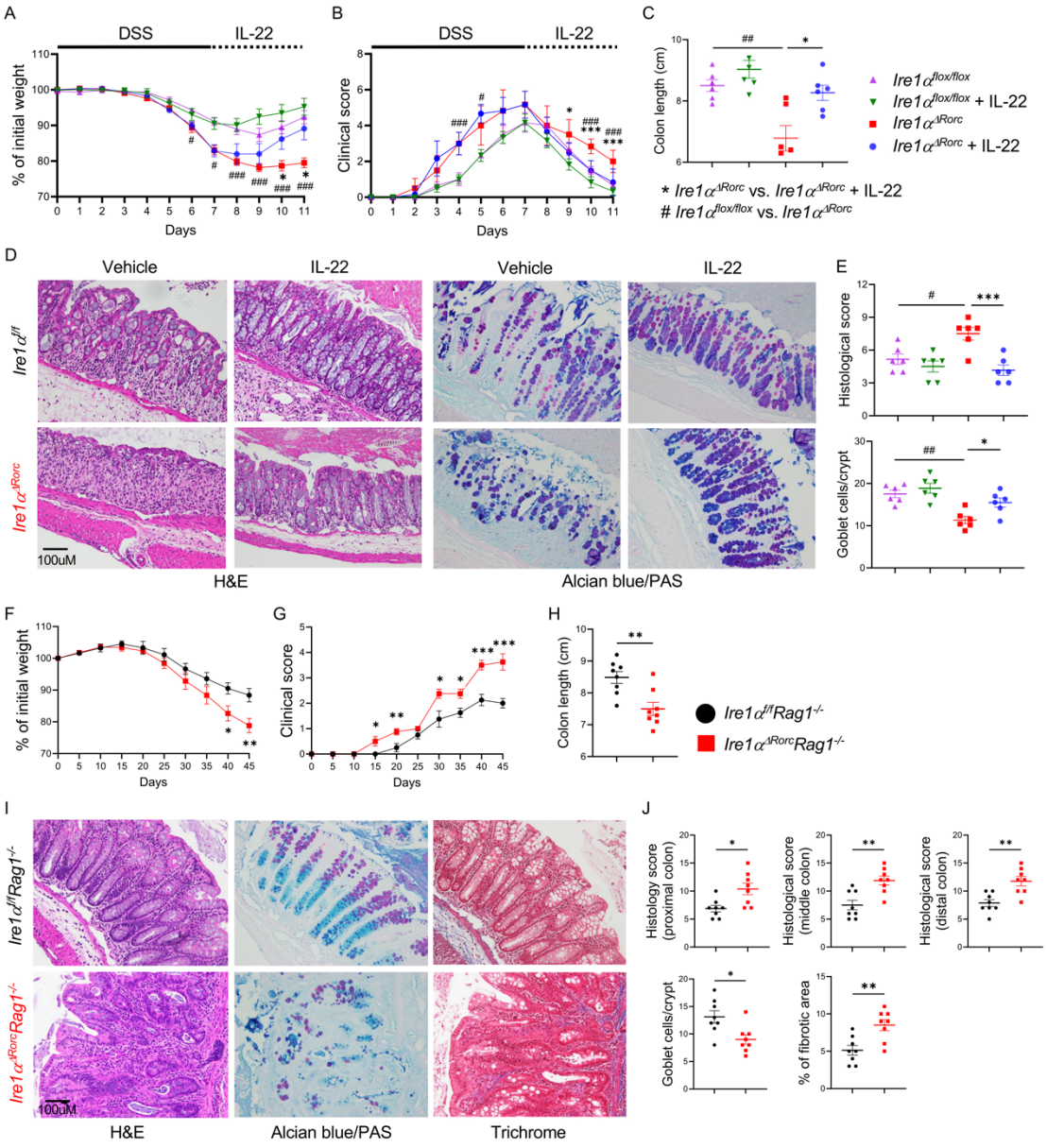

Figure 6: Loss of *Ire1α* in ILC3s impedes recovery from acute DSS colitis and exacerbates T-cell transfer-induced colitis. *Ire1α*$^{\Delta Rorc}$ mice were given 3.5% DSS in drinking water for 7 days to induce acute colitis, followed by intraperitoneal injection of 1 µg mouse recombinant IL-22 daily on days 7-11. (A) Weight loss and (B) clinical scores were measured daily. Mice were sacrificed on day 11 and colons harvested. We measured the following parameters: colon length (C); histology score determined by H&E staining (D, E); and goblet cell numbers assessed via alcian

blue/PAS staining (D, E) (n = 6). (F-J) Adoptive transfer of WT $CD4^{+}CD45RB^{hi}$ T cells to *Ire1α*$^{\Delta Rorc}$*Rag1*$^{-/-}$ and *Ire1α*$^{flox/flox}$*Rag1*$^{-/-}$ (control) littermates to induce chronic colitis. (F) Weight loss and (G) clinical scores were measured every 5 days. Mice were sacrificed on day 45 post-transfer and colons were harvested for measurement of length (H), H&E staining, alcian blue/PAS staining, and Masson's trichrome staining (I, J) (n = 8). Data represent 2 independent experiments. P values were calculated using 2-tailed Student t test or one-way ANOVA with Tukey's multiple comparisons test. Error bars indicate SEM. * or #p<0.05, ** or ##p<0.01, ***p<0.001.

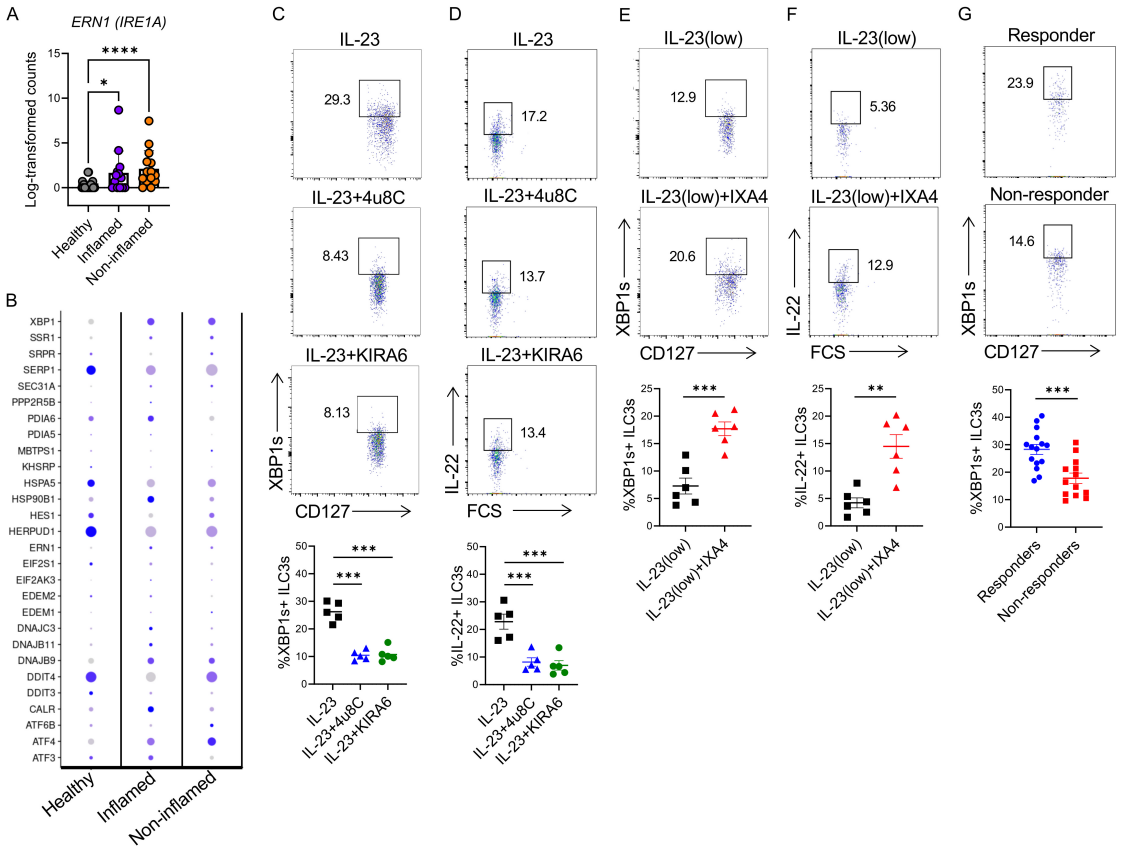

Figure 7: IRE1 modulators orchestrate cytokine production in human ILC3s; intestinal XBP1+ ILC3s positively correlate with response to ustekinumab in CD patients. (A) Expression of *ERN1* (*IRE1A*) in colonic ILC3s from healthy controls, inflamed and non-inflamed tissues of UC patients. (B) Expression of UPR genes in colonic ILC3s from healthy controls, inflamed and non-inflamed tissues of UC patients. (C-F) ILC3s were sort-purified from colonic biopsies collected from healthy individuals, treated as noted with IL-23 (10 ng/mL in C, D; 0.1 ng/mL in E, F), 10 μM 4μ8C, 1 μM KIRA6, or 10 μM IXA4 for 10 hours (with GolgiPlug for the last 4 hours), intracellular XBP1s (B, D) and IL-22 (C, E) was measured by flow cytometry (n = 5-6). Representative plots and the percentage of IL-22$^+$ ILC3s in each sample are shown. (G) ILC3s were isolated from inflamed mucosal biopsies collected from CD patients before starting ustekinumab, ILC3 markers and intracellular XBP1s were detected by flow cytometry. Representative plots are shown on the left and the percentage of XBP1s$^+$ ILC3s in each sample

shown on the right (total n = 28). P values were calculated using 2-tailed Student t test or one-way ANOVA with Tukey's multiple comparisons test. Error bars indicate SEM. *p<0.05, **p<0.01, ***p<0.001, ****p<0.0001.

References

1. Vivier E, Artis D, Colonna M, Diefenbach A, Di Santo JP, Eberl G, et al. Innate Lymphoid Cells: 10 Years On. *Cell.* 2018;174(5):1054-66.
2. Wang Q, Robinette ML, Billon C, Collins PL, Bando JK, Fachi JL, et al. Circadian rhythm-dependent and circadian rhythm-independent impacts of the molecular clock on type 3 innate lymphoid cells. *Sci Immunol.* 2019;4(40).
3. Teng F, Goc J, Zhou L, Chu C, Shah MA, Eberl G, et al. A circadian clock is essential for homeostasis of group 3 innate lymphoid cells in the gut. *Sci Immunol.* 2019;4(40).
4. Lyu MZ, Suzuki H, Kang L, Gaspal F, Zhou WQ, Goc J, et al. ILC3s select microbiota-specific regulatory T cells to establish tolerance in the gut. *Nature.* 2022;610(7933):744-+.
5. Kedmi R, Najar TA, Mesa KR, Grayson A, Kroehling L, Hao Y, et al. A RORgammat(+) cell instructs gut microbiota-specific T(reg) cell differentiation. *Nature.* 2022;610(7933):737-43.
6. Forkel M, van Tol S, Hoog C, Michaelsson J, Almer S, and Mjosberg J. Distinct Alterations in the Composition of Mucosal Innate Lymphoid Cells in Newly Diagnosed and Established Crohn's Disease and Ulcerative Colitis. *J Crohns Colitis.* 2019;13(1):67-78.
7. Hepworth MR, Fung TC, Masur SH, Kelsen JR, McConnell FM, Dubrot J, et al. Immune tolerance. Group 3 innate lymphoid cells mediate intestinal selection of commensal bacteria-specific CD4(+) T cells. *Science.* 2015;348(6238):1031-5.
8. Van Limbergen J, Radford-Smith G, and Satsangi J. Advances in IBD genetics. *Nat Rev Gastro Hepat.* 2014;11(6).
9. Graham DB, and Xavier RJ. Pathway paradigms revealed from the genetics of inflammatory bowel disease. *Nature.* 2020;578(7796):527-39.
10. Urra H, Pihan P, and Hetz C. The UPRosome - decoding novel biological outputs of IRE1alpha function. *J Cell Sci.* 2020;133(15).
11. Hetz C, Zhang KZ, and Kaufman RJ. Mechanisms, regulation and functions of the unfolded protein response. *Nat Rev Mol Cell Bio.* 2020;21(8):421-38.
12. Almanza A, Carlesso A, Chintha C, Creedican S, Doultsinos D, Leuzzi B, et al. Endoplasmic reticulum stress signalling - from basic mechanisms to clinical applications. *FEBS J.* 2019;286(2):241-78.
13. Kaser A, Lee AH, Franke A, Glickman JN, Zeissig S, Tilg H, et al. XBP1 links ER stress to intestinal inflammation and confers genetic risk for human inflammatory bowel disease. *Cell.* 2008;134(5):743-56.
14. Eri RD, Adams RJ, Tran TV, Tong H, Das I, Roche DK, et al. An intestinal epithelial defect conferring ER stress results in inflammation involving both innate and adaptive immunity. *Mucosal Immunology.* 2011;4(3):354-64.
15. Hasnain SZ, Tauro S, Das I, Tong H, Chen ACH, Jeffery PL, et al. IL-10 Promotes Production of Intestinal Mucus by Suppressing Protein Misfolding and Endoplasmic Reticulum Stress in Goblet Cells. *Gastroenterology.* 2013;144(2):357-+.
16. Das I, Png CW, Oancea I, Hasnain SZ, Lourie R, Proctor M, et al. Glucocorticoids alleviate intestinal ER stress by enhancing protein folding and degradation of misfolded proteins. *J Exp Med.* 2013;210(6):1201-16.
17. Cao SS, Zimmermann EM, Chuang BM, Song B, Nwokoye A, Wilkinson JE, et al. The unfolded protein response and chemical chaperones reduce protein misfolding and colitis in mice. *Gastroenterology.* 2013;144(5):989-1000 e6.
18. Cao SS, Wang M, Harrington JC, Chuang BM, Eckmann L, and Kaufman RJ. Phosphorylation of eIF2a Is Dispensable for Differentiation but Required at a Posttranscriptional Level for Paneth Cell Function and Intestinal Homeostasis in Mice. *Inflammatory Bowel Diseases.* 2014;20(4):712-22.

19. Kaser A, Adolph TE, and Blumberg RS. The unfolded protein response and gastrointestinal disease. *Semin Immunopathol.* 2013;35(3):307-19.
20. Hosomi S, Grootjans J, Tschurtschenthaler M, Krupka N, Matute JD, Flak MB, et al. Intestinal epithelial cell endoplasmic reticulum stress promotes MULT1 up-regulation and NKG2D-mediated inflammation. *J Exp Med.* 2017;214(10):2985-97.
21. Stengel ST, Fazio A, Lipinski S, Jahn MT, Aden K, Ito G, et al. Activating Transcription Factor 6 Mediates Inflammatory Signals in Intestinal Epithelial Cells Upon Endoplasmic Reticulum Stress. *Gastroenterology.* 2020;159(4):1357-+.
22. Coleman OI, and Haller D. ER Stress and the UPR in Shaping Intestinal Tissue Homeostasis and Immunity. *Front Immunol.* 2019;10:2825.
23. Godinho-Silva C, Domingues RG, Rendas M, Raposo B, Ribeiro H, da Silva JA, et al. Light-entrained and brain-tuned circadian circuits regulate ILC3s and gut homeostasis. *Nature.* 2019;574(7777):254-8.
24. Seillet C, Luong K, Tellier J, Jacquelot N, Shen RD, Hickey P, et al. The neuropeptide VIP confers anticipatory mucosal immunity by regulating ILC3 activity. *Nat Immunol.* 2020;21(2):168-77.
25. Yu HB, Yang H, Allaire JM, Ma C, Graef FA, Mortha A, et al. Vasoactive intestinal peptide promotes host defense against enteric pathogens by modulating the recruitment of group 3 innate lymphoid cells. *Proc Natl Acad Sci U S A.* 2021;118(41).
26. Pascal M, Kazakov A, Chevalier G, Dubrule L, Deyrat J, Dupin A, et al. The neuropeptide VIP potentiates intestinal innate type 2 and type 3 immunity in response to feeding. *Mucosal Immunol.* 2022;15(4):629-41.
27. Cao SS, and Kaufman RJ. Endoplasmic reticulum stress and oxidative stress in cell fate decision and human disease. *Antioxid Redox Signal.* 2014;21(3):396-413.
28. Di Luccia B, Gilfillan S, Cella M, Colonna M, and Huang SC. ILC3s integrate glycolysis and mitochondrial production of reactive oxygen species to fulfill activation demands. *J Exp Med.* 2019;216(10):2231-41.
29. Ball JA, Vlisidou I, Blunt MD, Wood W, and Ward SG. Hydrogen Peroxide Triggers a Dual Signaling Axis To Selectively Suppress Activated Human T Lymphocyte Migration. *J Immunol.* 2017;198(9):3679-89.
30. Gundu C, Arruri VK, Sherkhane B, Khatri DK, and Singh SB. GSK2606414 attenuates PERK/p-eIF2alpha/ATF4/CHOP axis and augments mitochondrial function to mitigate high glucose induced neurotoxicity in N2A cells. *Curr Res Pharmacol Drug Discov.* 2022;3:100087.
31. Zhang K, Wang S, Malhotra J, Hassler JR, Back SH, Wang G, et al. The unfolded protein response transducer IRE1alpha prevents ER stress-induced hepatic steatosis. *EMBO J.* 2011;30(7):1357-75.
32. Nagao-Kitamoto H, Leslie JL, Kitamoto S, Jin C, Thomsson KA, Gillilland MG, 3rd, et al. Interleukin-22-mediated host glycosylation prevents Clostridioides difficile infection by modulating the metabolic activity of the gut microbiota. *Nat Med.* 2020;26(4):608-17.
33. Fachi JL, Secca C, Rodrigues PB, Mato FCP, Di Luccia B, Felipe JS, et al. Acetate coordinates neutrophil and ILC3 responses against C. difficile through FFAR2. *J Exp Med.* 2020;217(3).
34. Peng V, Jaeger N, and Colonna M. Innate Lymphoid Cells and Inflammatory Bowel Disease. *Adv Exp Med Biol.* 2022;1365:97-112.
35. Silberger DJ, Zindl CL, and Weaver CT. Citrobacter rodentium: a model enteropathogen for understanding the interplay of innate and adaptive components of type 3 immunity. *Mucosal Immunol.* 2017;10(5):1108-17.
36. Satoh-Takayama N, Vosshenrich CAJ, Lesjean-Pottier S, Sawa S, Lochner M, Rattis F, et al. Microbial Flora Drives Interleukin 22 Production in Intestinal NKp46(+) Cells that Provide Innate Mucosal Immune Defense. *Immunity.* 2008;29(6):958-70.

37. Zheng Y, Valdez PA, Danilenko DM, Hu Y, Sa SM, Gong Q, et al. Interleukin-22 mediates early host defense against attaching and effacing bacterial pathogens. *Nature Medicine.* 2008;14(3):282-9.
38. Sonnenberg GF, Monticelli LA, Elloso MM, Fouser LA, and Artis D. CD4(+) Lymphoid Tissue-Inducer Cells Promote Innate Immunity in the Gut. *Immunity.* 2011;34(1):122-34.
39. Secca C, Bando JK, Fachi JL, Gilfillan S, Peng V, Di Luccia B, et al. Spatial distribution of LTi-like cells in intestinal mucosa regulates type 3 innate immunity. *Proc Natl Acad Sci U S A.* 2021;118(23).
40. Ostanin DV, Bao J, Koboziev I, Gray L, Robinson-Jackson SA, Kosloski-Davidson M, et al. T cell transfer model of chronic colitis: concepts, considerations, and tricks of the trade. *Am J Physiol Gastrointest Liver Physiol.* 2009;296(2):G135-46.
41. Li H, Song J, Niu G, Zhang H, Guo J, Shih DQ, et al. TL1A blocking ameliorates intestinal fibrosis in the T cell transfer model of chronic colitis in mice. *Pathol Res Pract.* 2018;214(2):217-27.
42. Smillie CS, Biton M, Ordovas-Montanes J, Sullivan KM, Burgin G, Graham DB, et al. Intra- and Inter-cellular Rewiring of the Human Colon during Ulcerative Colitis. *Cell.* 2019;178(3):714-30 e22.
43. Zhang D, De Veirman K, Fan R, Jian Q, Zhang Y, Lei L, et al. ER stress arm XBP1s plays a pivotal role in proteasome inhibition-induced bone formation. *Stem Cell Res Ther.* 2020;11(1):516.
44. Hassler JR, Scheuner DL, Wang S, Han J, Kodali VK, Li P, et al. The IRE1alpha/XBP1s Pathway Is Essential for the Glucose Response and Protection of beta Cells. *PLoS Biol.* 2015;13(10):e1002277.
45. Madhavan A, Kok BP, Rius B, Grandjean JMD, Alabi A, Albert V, et al. Pharmacologic IRE1/XBP1s activation promotes systemic adaptive remodeling in obesity. *Nat Commun.* 2022;13(1):608.
46. Cross BCS, Bond PJ, Sadowski PG, Jha BK, Zak J, Goodman JM, et al. The molecular basis for selective inhibition of unconventional mRNA splicing by an IRE1-binding small molecule. *P Natl Acad Sci USA.* 2012;109(15):E869-E78.
47. Ghosh R, Wang L, Wang ES, Perera BG, Igbaria A, Morita S, et al. Allosteric inhibition of the IRE1alpha RNase preserves cell viability and function during endoplasmic reticulum stress. *Cell.* 2014;158(3):534-48.
48. Grandjean JMD, Madhavan A, Cech L, Seguinot BO, Paxman RJ, Smith E, et al. Pharmacologic IRE1/XBP1s activation confers targeted ER proteostasis reprogramming. *Nat Chem Biol.* 2020;16(10):1052-+.
49. Cao SY, Cella M, Jaeger N, Ciorba M, Escudero GO, Gutierrez A, et al. Mass Cytometry Analysis of Crohn's Disease-Like Phenotype of the Ileoanal Pouch Following Ileal Pouch-Anal Anastomosis for Ulcerative Colitis. *Gastroenterology.* 2022;162(3):S58-S9.
50. Khalaf K, Tornese P, Cocco A, and Albanese A. Tauroursodeoxycholic acid: a potential therapeutic tool in neurodegenerative diseases. *Transl Neurodegener.* 2022;11(1):33.
51. Martinon F, Chen X, Lee AH, and Glimcher LH. TLR activation of the transcription factor XBP1 regulates innate immune responses in macrophages. *Nat Immunol.* 2010;11(5):411-8.
52. Cretenet G, Le Clech M, and Gachon F. Circadian clock-coordinated 12 Hr period rhythmic activation of the IRE1alpha pathway controls lipid metabolism in mouse liver. *Cell Metab.* 2010;11(1):47-57.
53. Cao Y, Trillo-Tinoco J, Sierra RA, Anadon C, Dai W, Mohamed E, et al. ER stress-induced mediator C/EBP homologous protein thwarts effector T cell activity in tumors through T-bet repression. *Nat Commun.* 2019;10(1):1280.
54. Klose CS, Kiss EA, Schwierzeck V, Ebert K, Hoyler T, d'Hargues Y, et al. A T-bet gradient controls the fate and function of CCR6-RORgammat+ innate lymphoid cells. *Nature.* 2013;494(7436):261-5.
55. Fiancette R, Finlay CM, Willis C, Bevington SL, Soley J, Ng STH, et al. Reciprocal transcription factor networks govern tissue-resident ILC3 subset function and identity. *Nat Immunol.* 2021;22(10):1245-55.

56. Schmitt H, Neurath MF, and Atreya R. Role of the IL23/IL17 Pathway in Crohn's Disease. *Frontiers in Immunology.* 2021;12.
57. Sewell GW, and Kaser A. Interleukin-23 in the Pathogenesis of Inflammatory Bowel Disease and Implications for Therapeutic Intervention. *J Crohns Colitis.* 2022;16(Supplement_2):ii3-ii19.
58. Sands BE, Chen J, Feagan BG, Penney M, Rees WA, Danese S, et al. Efficacy and Safety of MEDI2070, an Antibody Against Interleukin 23, in Patients With Moderate to Severe Crohn's Disease: A Phase 2a Study. *Gastroenterology.* 2017;153(1):77-86 e6.
59. Eberl G, and Littman DR. Thymic origin of intestinal alphabeta T cells revealed by fate mapping of RORgammat+ cells. *Science.* 2004;305(5681):248-51.
60. Fachi JL, Pral LP, Dos Santos JAC, Codo AC, de Oliveira S, Felipe JS, et al. Hypoxia enhances ILC3 responses through HIF-1alpha-dependent mechanism. *Mucosal Immunol.* 2021;14(4):828-41.
61. Fachi JL, Pral LP, Assis HC, Oliveira S, Rodovalho VR, Dos Santos JAC, et al. Hyperbaric oxygen augments susceptibility to C. difficile infection by impairing gut microbiota ability to stimulate the HIF-1alpha-IL-22 axis in ILC3. *Gut Microbes.* 2024;16(1):2297872.
62. Peng V, Cao SY, Trsan T, Bando JK, Avila-Pacheco J, Cleveland JL, et al. Ornithine decarboxylase supports ILC3 responses in infectious and autoimmune colitis through positive regulation of IL-22 transcription. *P Natl Acad Sci USA.* 2022;119(45).
63. Bando JK, Gilfillan S, Song C, McDonald KG, Huang SC, Newberry RD, et al. The Tumor Necrosis Factor Superfamily Member RANKL Suppresses Effector Cytokine Production in Group 3 Innate Lymphoid Cells. *Immunity.* 2018;48(6):1208-19 e4.
64. Raczynski AR, Muthupalani S, Schlieper K, Fox JG, Tannenbaum SR, and Schauer DB. Enteric infection with Citrobacter rodentium induces coagulative liver necrosis and hepatic inflammation prior to peak infection and colonic disease. *PLoS One.* 2012;7(3):e33099.
65. Uddin J, Tomar S, Sharma A, Waggoner L, Ganesan V, Marella S, et al. PIR-B Regulates CD4(+) IL17a(+) T-Cell Survival and Restricts T-Cell-Dependent Intestinal Inflammatory Responses. *Cell Mol Gastroenterol Hepatol.* 2021;12(4):1479-502.
66. Eri R, McGuckin MA, and Wadley R. T cell transfer model of colitis: a great tool to assess the contribution of T cells in chronic intestinal inflammation. *Methods Mol Biol.* 2012;844:261-75.
67. Love MI, Huber W, and Anders S. Moderated estimation of fold change and dispersion for RNA-seq data with DESeq2. *Genome Biol.* 2014;15(12):550.
68. Yu G, Wang LG, Han Y, and He QY. clusterProfiler: an R package for comparing biological themes among gene clusters. *OMICS.* 2012;16(5):284-7.